Journal of Power Sources 189 (2009) 66–71

Contents lists available at ScienceDirect

Journal of Power Sources

journal homepage: www.elsevier.com/locate/jpowsour

Investigation of solid electrolyte interfacial layer development during continuous cycling using ac impedance spectra and micro-structural analysis

P.L. Moss[a], G. Au[b], E.J. Plichta[b], J.P. Zheng[a,c,*]

[a] Department of Electrical and Computer Engineering, Florida A&M University and Florida State University, Tallahassee, FL 32310, United States
[b] U.S. Army CERDEC, Ft. Monmouth, NJ 07703, United States
[c] Center for Advance Power Systems, Florida State University, Tallahassee, FL 32310, United States

ARTICLE INFO

Article history:
Received 26 June 2008
Received in revised form 15 October 2008
Accepted 13 November 2008
Available online 21 November 2008

Keywords:
Solid-electrolyte interfacial layer
ac Impedance
Cycling performance
Lithium polymer battery

ABSTRACT

The formation of passivating surface films on the electrodes of a lithium-ion polymer battery was investigated at various cycling state using ac impedance spectroscopy and scanning electron microscopy (SEM). A sealed commercial cell (Sony Co.) with a nominal capacity of 840 mAh was used for the experiment. An equivalent circuit used to model the impedance spectra show that, with continuous cycling there is a relatively large increase in the interfacial impedance and charge transfer resistances after a few hundred charge–discharge cycles. It was observed that the cell capacity decrease with increase cell impedance. SEM analysis on the electrodes shows that during continuous charge–discharge cycling, the deposition of sub-micro-size particles and dissolution of surface films on the graphite surface. This observation is consistent with increase in cell impedance as a function of charge/discharge cycling.

1. Introduction

Lithium-ion polymer batteries are widely used in small portable devices such as mobiles phones, notebook computers and personal digital assistant, however due to their relatively high energy density it has been proposed for use in high energy density and large scale applications such in hybrid and hybrid electric vehicles [1–4]. Extensive studies have shown that solvent decomposition, exfoliation of the electrode material, and co-intercalation phenomena plays a major role in the irreversible capacity lost with continuous intercalation/de-intercalation of lithium-ions (Li^+). Additionally, passivation of the electrodes by surface films upon initial insertion of Li^+ into the negative graphite electrode result in the thermodynamic stabilization of the electrodes which prevents further reaction with the solution species. SEI also plays the critical role in blocking the passage of electrons and preventing the co-intercalation of organic species from the electrolyte while allowing the conduction of Li^+.

The formation of SEI and its influence on cell performance have been extensively studied. Many techniques including Fourier transform infrared spectroscopy, X-ray photoelectron spectroscopy, in situ atomic force microscopy, and scanning electron microscopy (SEM) have been employed to characterize and provide valuable information about the nature of SEI. The properties and chemical makeup of SEI have been the study of intense scientific investigations with analysis [5,6] showing that the major constituents of these complex surface films in alkyl carbonate solution are $ROCO_2Li$, ROLi, RCOOLi, LiCl, LiF, and Li_2CO_3; the continuous precipitation of these surface films on the electrodes are also one of the main reasons for irreversible capacity loss in lithium-ion batteries. Reports have shown that the formation of SEI on the graphite electrode is strongly dependent on the composition of the electrolyte and the graphite structure and plays a critical role in the electrochemical performance [7].

Appetecchi et al. [8] have studied the interfacial behavior of Li_xC_6 electrode and $LiClO_4$-EC-DMC-Pan polymer electrolyte with Li as reference electrode. ac Impedance spectroscopy shows two separate semi-circles in the high to medium frequency range and a Warburg behavior in the low frequency range. The electronic resistance was ascribed to the left intersect of the two semi-circles and the medium-low frequency semi-circle was ascribed to passivation of the electrode by reaction between the Li_xC_6 electrode and the polymer electrolyte. Cycling study was also carried out on the positive electrode for which the initial capacity was not retained with cycling. It was concluded that this lost in capacity in the positive electrode was due to lost in structural integrity or reduction of solution species on the surface of the electrode. Kim et al. [9] conclude a similar study for which they investigated the electrochemical performance of Li-ion polymer battery consisting $Li_{1-x}CoO_2$ as cathode, mesocarbon microbead as anode and

* Corresponding author at: Department of Electrical and Computer Engineering, Florida A&M University and Florida State University, Tallahassee, FL 32310, United States.
E-mail address: zheng@eng.fsu.edu (J.P. Zheng).

0378-7753/$ – see front matter © 2008 Elsevier B.V. All rights reserved.
doi:10.1016/j.jpowsour.2008.11.048

P(VdF-*co*-HFP) based gel polymer electrolyte. They show a reduction in coulombic efficiency from 99% to 98.5% in the 1st and 20th cycles, respectively. They also ascribed the decrease in capacity and increase in internal impedance to the physical changes at the electrode/electrolyte interface as a result of electrolyte decomposition or change in the electrode structure.

The present study investigates the cycling characteristic and performance of lithium-ion polymer cell (Li_xC_6/solid polymer electrolyte (SPE)/$Li_{1-x}CoO_2$) using electrochemical impedance spectroscopy. In addition, morphological analysis will be used along with EIS to understand the formation of SEI with continuous charge–discharge cycling.

2. Experimental

The lithium-polymer battery used in this experiment is a commercial cell with a nominal discharge capacity of 840 mAh as specified by the manufacture (Sony co.). The cell had an aluminum plastic laminated exterior film with dimensions 38 mm × 35 mm × 62 mm. The cell structure consists of Cu foil|graphite negative electrode|porous polyethylene separator, gel solution of ethylene carbonate (EC)/propylene carbonate (PC), $LiPF_6$|$LiCoO_2$ positive electrode|Al foil. The cell was galvanostatically/potentiostatically cycled in a two-electrode configuration. The cell was charge and discharge in a constant current (CC) and constant voltage (CV) mode at room temperature using an Arbin battery tester. For continuous cycling the cell was charged using a CC protocol to an upper potential of 4.2 V then using CV protocol until the current dropped to less than 10 mA; the cell was then discharged to a lower cutoff potential of 3.0 V using the CC protocol.

EIS measurements were carried out using a solartron 1250B frequency response analyzer with windows PC control and data acquisition software by zplot (Snibber Associates). EIS measurements were performed at various levels of Li-ion intercalation as well as for cells in the continuous cycled state. The corresponding spectra result was then evaluated by fitting the electrode response to an equivalent circuit using Zview software (Scribner Associates). All spectra were collected using a 5 mV sinusoidal stimulus with frequency ranging from 10 mHz to 20 kHz. In addition the spectra was collected under open-circuit voltage (OCV) conditions where CC–CV protocol is applied; in this mode the cell was charged using CC to the desired OCV then a CV is applied and held at equilibrium until the current decayed to less than 10 mA. The surface morphology was studied using a SEM, Joel JSM 5900 operated at 20 keV.

3. Results and discussions

3.1. Electrochemical impedance spectroscopy

Fig. 1 shows the result of the typical impedance spectra for an uncycled cell measured at an OCV of 3.6 V. The impedance in the complex plane represents the combine contribution from both anode and cathode, therefore all parameters related to mass and charge transport reflects the superposition of both electrodes. The spectra contain a resistance R_s at the interception of the real axis which can be ascribed to the electrolyte, separator and contacts, and correlates with the ohmic polarization of the cell. The spectra show an inductive tail at high frequencies (20–15.85 kHz) for which previous reports [10,11] have attributed to the porosity of the electrodes and jelly-roll structure of the cell, however some inductive behavior have been observed when conducting EIS on the leads connected to the frequency response analyzer, suggesting that the leads used to measure spectra data may contribute to some of the inductive behavior. At least three overlapping depressed semi-cycles

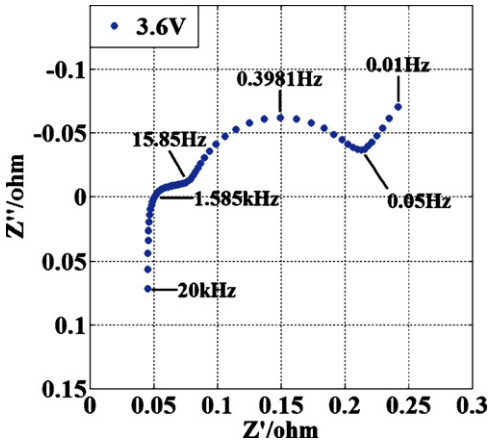

Fig. 1. Typical Nyquist plot for new cell perform at OCV of 3.6 V.

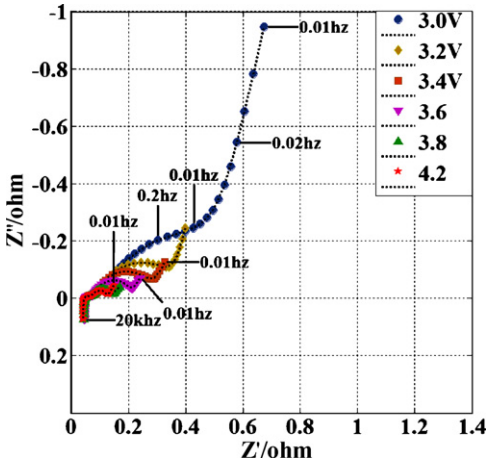

Fig. 2. Comparison of the experimental and fitted spectra for Li-ion polymer cell at various potential voltages of (●) 3.0 V; (♦) 3.2 V; (■) 3.4 V; (▼) 3.6 V; (▲) 3.8 V; (⋆) 4.2 V in a frequency range of 0.01 Hz to 20 kHz.

is observed at high to medium frequencies (1.585 kHz–15.85 Hz). These semi-cycles are associated with the migration of lithium ion through SEI layers which covers the electrode and have equivalent SEI resistance R_f and corresponding SEI capacitance C_f. The semi-circle at mid-frequencies (15.85–0.05 Hz) are associated with

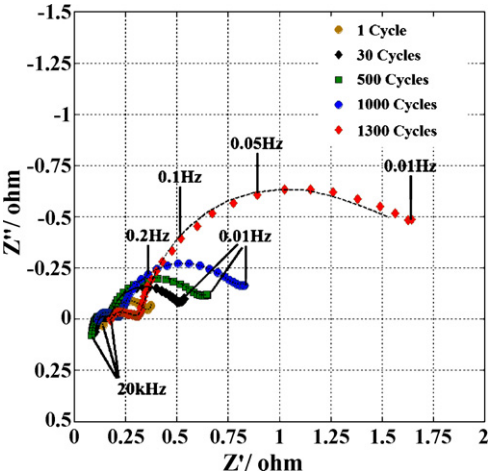

Fig. 3. Nyquist plots at various cycling states for experimental and fitted spectra data obtain from the equivalent circuit, all data collected at OCV of 3.6 V.

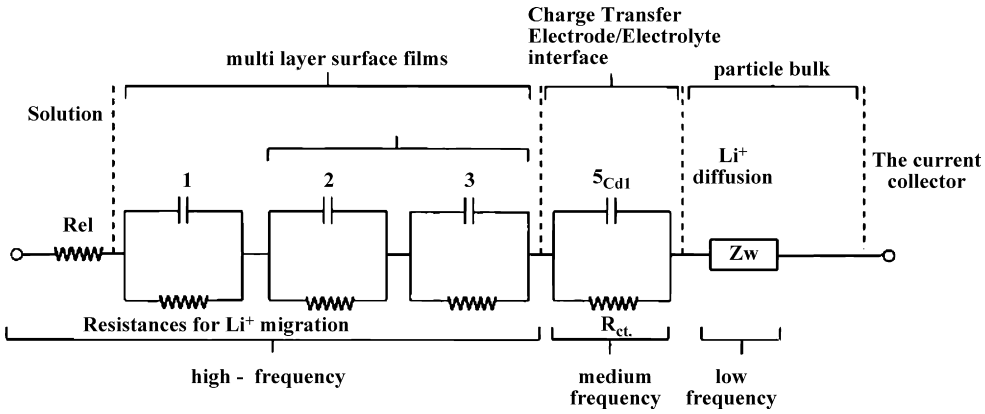

Fig. 4. Equivalent circuit used in the interpretation of the impedance spectra data.

intercalation type reactions and is characterized by charge transfer resistance R_{ct} and the associated double-layer capacitance C_{dl}. The low frequency (0.05–0.01 Hz) Warburg slope line represents the semi-infinite diffusion of Li-ion in the electrodes.

The impedance spectrum collected from an uncycled cell in the potential range 4.2–3.0 V is shown in Fig. 2. It is observed that the ohmic resistance R_{el}, show little variation with various levels of Li-ion intercalation. The low frequency semi-cycle associated with the charge transfer kinetics shows the largest increase with decreasing polarization potential. This is attributed to the availability of effective reactive sited for Li-ion during intercalation/de-intercalation [12,13]. The depress high frequency semi-cycle show some moderated increase when the cell potential decreasing to less than 3.6 V. This is a result of volume changes [14] during de-intercalation/intercalation resulting in the expansion–contraction in the cross-sectional area of the SEI. The overall increase in the impedances at low potentials also indicated some level of difficulty in the electrochemical kinetics.

In order to elucidate the decrease in cell performance of continuous cycled cells, ac impedance spectroscopy was conducted at various cycling number. Fig. 3 shows the impedance spectrum obtained at 1, 30, 500, 1000 and 13,000 charge–discharge cycles. The spectrums were all obtained at an OCV of 3.6 V. It is observed that after 300 charge–discharge cycles, an increase in the impedance of the high frequency (i.e. 20 kHz to 20 Hz at 300 cycles) regions of the spectrum. This indicates a decrease in the ionic conductivity of the SEI layer. In addition, an increase in the size of the mid-frequency semi-circle indicates a slowing down of the electrochemical reactions at the electrode–electrolyte interface. The low frequency Warburg slope that appeared during initial cycling had shifted to lower frequencies after a few hundred charge–discharge cycles. This suggests an increase in rate limiting time constant associated with other processes involved in the cell reaction. It can also be observed that the inductive arc diminishes with prolong cycling which may indicates that some change in the porosity (i.e. formation of a compact layer) at the electrode–electrolyte interface.

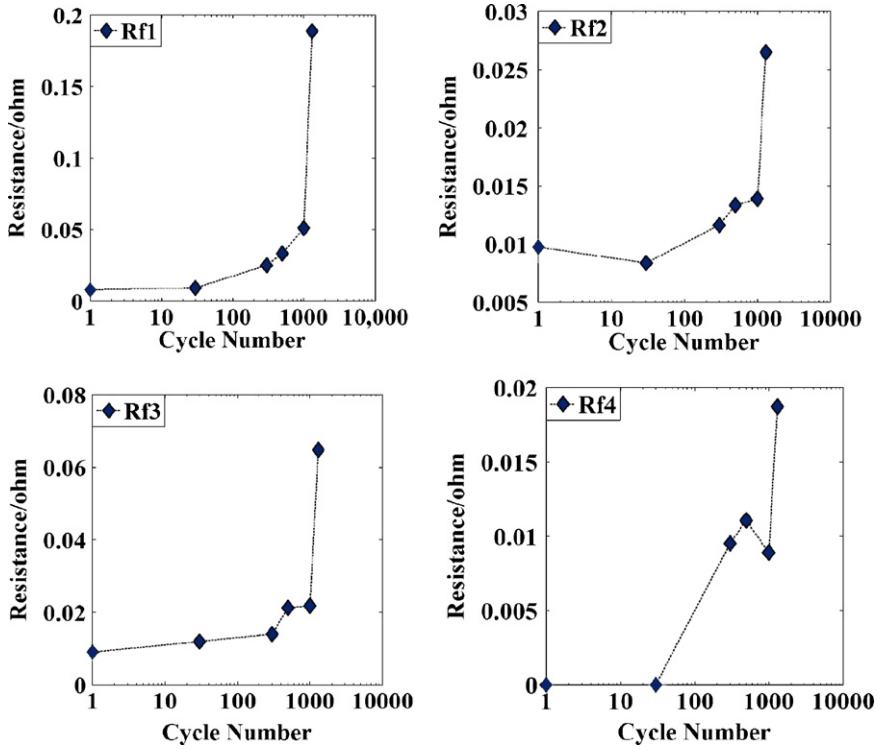

Fig. 5. Surface film resistance values obtained by fitting experiment data using equivalent circuit.

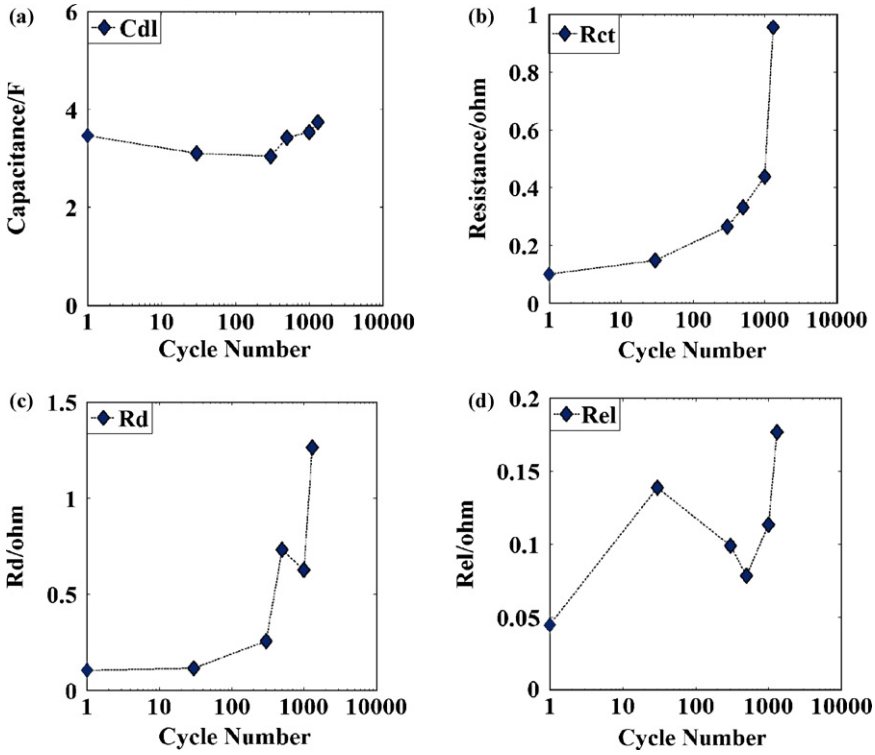

Fig. 6. Parameters obtained at different cycling number: (a) double-layer capacitance, C_{dl}; (b) charge transfer resistance, R_{ct}; (c) mass transport resistance, R_d; (d) ohmic resistance, R_{el}.

3.2. Equivalent circuit model

Fig. 4 depicts the modified Randles equivalent circuit commonly used to simulate the impedance response of a battery. The optimum parameters in the circuit were determined by the method of non-linear least square (NLLS) fitting procedure. From this circuit a good fit is achieved, and shown by the solid lines in the complex plot, Figs. 2 and 3. The resistance R_{el} represents the ohmic impedance and is seen at the interception of the real axis at the high frequency end of the complex plot; the relative time constants attributing to the passive surface films are observed at the high frequency end of the spectra. The combined resistive and capacitive behavior of

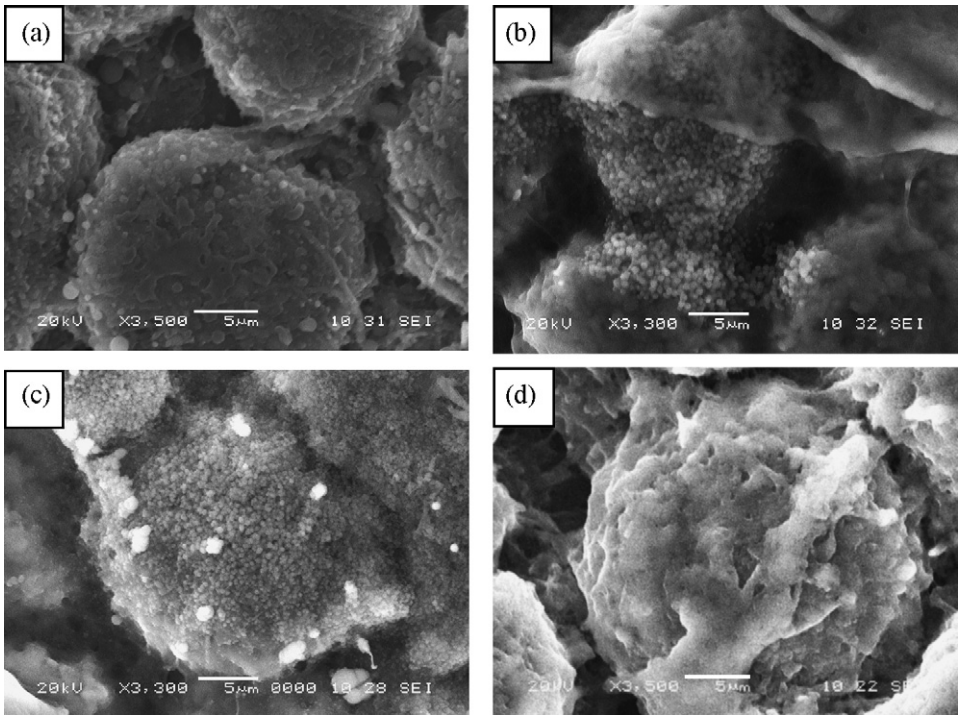

Fig. 7. SEM micrograph of the anode (Li_xC_6) from (a) new cell, (b) after 30 cycles, (c) after 300 cycles, and (d) 1300 cycles.

the passive surface films on the anode and cathode is represented by a series connection of three to four parallel RC circuit elements dependent on the cycling number; the charge-transfer kinetics at the electrode–electrolyte interface is represented by a parallel resistor R_{ct} (charge-transfer resistance) and capacitor C_{dl} (double-layer capacitance); the solid state diffusion of lithium-ion into the bulk electrode at low frequencies is represented by the Warburg element Z_w given by the following equation [15]:

$$Z_w = \frac{\tau_d}{C_d} \frac{\coth(j\omega\tau_d)^p}{(j\omega\tau_d)^p} \quad (1)$$

where ω is related to the angular frequency of the applied ac signal, τ_d is associated with the characteristic diffusion time constant, C_d the differential capacitance associated with the intercalation process at low frequencies and p denotes the finite space behavior or porosity of the electrode [16,17]. In addition the ionic resistance can be expressed in the following form Fig. 5:

$$R_d = \frac{\tau_d}{C_d} \quad (2)$$

Next the relationship between different cycling stages and the interpretation of various circuit parameters are obtained from the equivalent circuit. Fig. 6(a)–(d) reveals that the values for SEI film impedances, charge transfer resistance and mass transfer resistance steadily increase with continuous charge–discharge cycling. From these plots several important observations can be made. First, are the parameters associated with the Li-ion conductivity through the surface films, which show significant increase in resistance R_f after 1300 charge–discharge cycles. The resistance increase is believed due to two facts: (1) continuous decomposition of solution species on the electrode surface with charge–discharge cycling; (2) the ionic resistance increased because the Li-ion concentration in electrolyte decreased with continuous cycling, and Li-ions were deposited on SEI layer [18–21]. This observation is consistence with the increase diameter of the high frequency semi-circles observed in the impedance spectra of the continuous cycled cell. Secondly, Fig. 6(b)–(c) shows that R_d and R_{ct} which are associated with mass and charge transport increase from 0.11 to 1.3 Ω and 0.099 to 0.96 Ω, respectively. Note that, R_{ct} is proportional to $1/i_0$, where i_0 is the rate limiting exchange current density [22–24]. Therefore, the increase in R_{ct} with continuous cycling indicates a corresponding decrease in i_0 which is associated with slow kinetic rates. Furthermore, the increase in ionic resistance R_d could due to several reasons including the consumption of Li-ion in the electrolyte, reduction in porosity of the electrode, or the diffusion channel being blocked within the crystal structure. In general it is observed that the overall impedance of the cell increase with increasing cycling number as a result of the decrease ionic conductivity of the SEI. The reduction in transport properties contributes to increase over-potential resulting in reduce rate capability of the cell which contributes greatly to reduce cell performance. Finally, ohmic resistance, R_{el}, in generally increased with increasing cycle number; however, a big jump at 30 cycles could be due to the experimental error such as bad contact. The increase in R_{el} with continuous cycling could be due to several factors including electrolyte degradation, electrode particles contact, and electrode-current collector contact.

3.3. Scanning electron microscopy (SEM)

SEM analysis was conducted on samples taken from the cathode ($Li_{1-x}CoO_2$) and anode electrode (Li_xC_6) to observe morphological changes at the electrode–electrolyte interface after prolong cycling. The electrode samples in the discharge state were collected in an ultrapure argon filled glove-box which included a sample from an uncycled cell, samples from cells that were cycled 30, 300, and 1300 cycles. Fig. 7(a)–(d) shows the SEM micrographs for

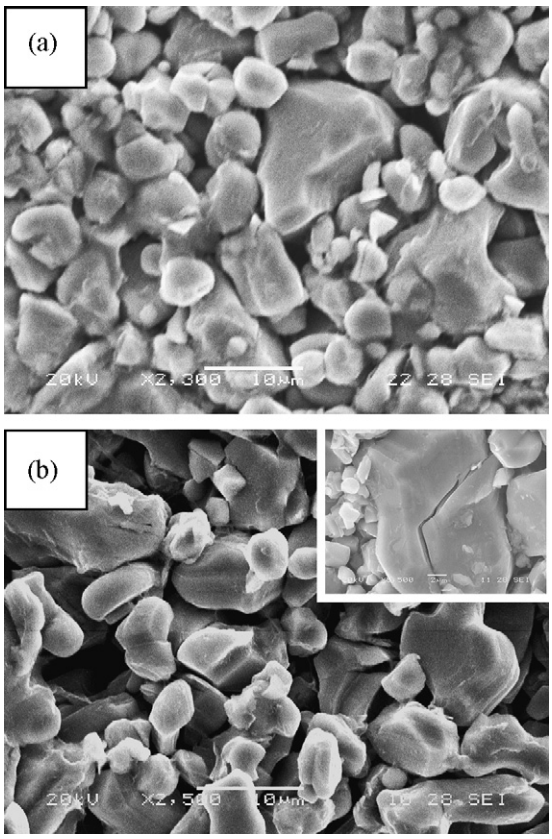

Fig. 8. SEM micrograph of the cathode ($Li_{1-x}CoO_2$) obtained from (a) new cell and (b) after 1300 cycles. A crack line was shown in insert.

the uncycled and continuous-cycled anode electrodes. The analysis of an uncycled cell show that the graphite electrode structure is composed single particle of mesocarbon microbeads (MCMB) of varying sizes (>10 μm). The observed morphological differences between the graphite electrodes before and after cycling show distinct changes. SEM analysis on the cell after prolong cycling (over 30 cycles) shows that surface films composing sub-micro-sized particles (Island growth) begin to deposited on the carbon electrode and significantly increase by the 300th cycle. After 1300 charge–discharge cycles, it can be seen, Fig. 7(d), that the surface of the carbon electrode becomes covered in a thick layer of passive surface film which acts to block the micropores for Li-ion transport. This observation is consistent with the conclusion from the ac impedance analysis which shows the hindrance of Li-ion transport through SEI. These surface films are the result of continuous reduction of the constituent from the electrolyte and salt species on the surface of the electrode which eventually leads to increase SEI impedance on the graphite electrode resulting in reduce cell performance with continuous cycling. SEM analysis of the cathode electrode ($Li_{1-x}CoO_2$) before and after cycling, Fig. 7(a) and (b) shows large irregular shaped particles of varying sizes. The micrographs reveal no observable change in surface morphology between the new and continuous cycled cell however some particles, Fig. 8(b) shows the development cracks. It is believe that the crack in the cathode electrode maybe due to mechanical strain during change-discharge cycling.

4. Conclusion

A sealed Li-ion polymer cell was investigated using ac impedance spectroscopy and SEM during continuous cycling and was fitted to an equivalent circuit to estimate cell parameter

with cycling. The resulting EIS data fitted to an equivalent circuit indicates an increase in interfacial resistance which plays a very important role in the rate of Li intercalation and is critical in determining cell efficiencies and reversible performance with continuous charge–discharge cycling. SEM analysis confirms that the anode is the only electrode that development surface films during continuous cycling. Therefore the increase in surface film impedance can be attributed the increase SEI layer on the anode surface. In addition some particles on the positive electrode ($Li_{1-x}CO_2$) show cracking with cycling which may be the result of structural stress. It is believed that a major increase in interfacial resistance on lithium polymer cells is related to the reduction of electrolyte species on the carbon electrode.

Acknowledgement

This work was supported by U.S. Army CERDEC and National Science Foundation ERC Program.

References

[1] Z. Chen, Q. Wang, K. Amine, Electrochimica Acta 51 (2006) 3890.
[2] Z. Ogumi, T. Abe, T. Fukutsuka, S. Yamate, Y. Iriyama, Journal of Power Sources 127 (2004) 72.
[3] T. Doi, Y. Iriyama, T. Abe, Z. Qgumi, Journal of Power Sources 142 (2005) 329.
[4] Y. Matoba, S. Matsui, M. Tabuchi, T. Sakai, Journal of Power Sources 137 (2004) 284.
[5] W. Van Schalkwijk, B. Scrosati, Advances in Lithium-ion Batteries, Kluwer Academic/Plenum Publishers, New York, NY, 2002, p. 36.
[6] S. Zhang, M.S. Ding, K. Xu, J. Allen, T.R. Jow, Electrochemical and Solid-State Letters 4 (2001) A206.
[7] L.J. Fu, H. Lui, C. Li, Y.P. Wu, E. Rahm, R. Holze, H.Q. Wu, Solid State Sciences 8 (2006) 113.
[8] G.B. Appetecchi, F. Croce, R. Marassi, L. Persi, P. Romagnoli, Electrochemica Acta 45 (1999) 23.
[9] H.-S. Kim, P. Periasamy, S.-I. Moon, Journal of Power Sources 141 (2005) 293.
[10] D. Zhou, Z. Lui, X. Lv, G. Zhou, J. Yin, Electrochemica Acta 51 (2006) 5731.
[11] N. Shalini Rodrigues, A. Munichandraiah, k. Skukla, Journal of Solid State Electrochemistry 3 (1999) 397.
[12] T. Abe, H. Fukuda, Y. Iriyama, Z. Ogumi, Journal of the Electrochemical Society 151 (2004) A1120.
[13] T. Abe, K. Takeda, T. Fukutsuka, Y. Iriyama, Z. Ogumi, Journal of the Electrochemical Society 151 (2004) C694.
[14] P. Ramadass, B.H. Parthasarathy, M. Gomadam, Ralph White, B.N. Popv, Journal of the Electrochemical Society 151 (2004) A196.
[15] M.D. Levi, G. Salitra, B. Markovsky, H. Teller, D. Aurbach, U. Heider, L. Heider, Journal of the Electrochemical Society 146 (1999) 1279.
[16] M.D. Levi, Z. Lu, D. Aurbach, Solid State Ionics 143 (2001) 309.
[17] H. Gabrisch, R. Yazami, B. Fultz, Journal of Power Sources (2003) 119–121, 674.
[18] M.-S. Zheng, Q.-F. Dong, H.-Q. Cai, M.-G. Jin, Z.-G. Lin, S.-G. Sun, Journal of the Electrochemical Society 152 (2005) A2207.
[19] T. Yoshida, M. Takahashi, S. Morikawa, C. Ihara, H. Katsukawa, T. Shiratsuchi, J.-I. Yamaki, Journal of the Electrochemical Society 153 (3) (2006) A576–A582.
[20] J. Christensen, J. Newman, Journal of the Electrochemical Society 150 (11) (2003) A1416–A1420.
[21] K. Kwon, F. Kong, F. Mclarnon, J.W. Evans, Journal of the Electrochemical Society 150 (2003) A229.
[22] S. Yang, H. Song, X. Chen, Electrochemistry Communications 8 (2006) 137.
[23] J. Yao, G.X. Wang, J.-H. Ahn, H.K. Lui, S.X. Dou, Journal of Power Sources 114 (2003) 292.
[24] V. Ganesh Kumar, N. Munichandraiah, A.K. Shukla, Journal of Applied Electrochemistry 27 (1997) 43.